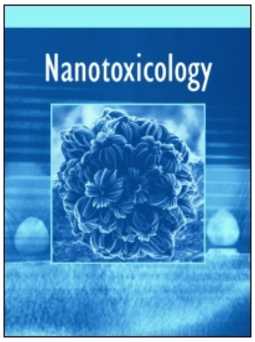

Nanotoxicology

ISSN: 1743-5390 (Print) 1743-5404 (Online) Journal homepage: http://www.tandfonline.com/loi/inan20

# Acute in vitro and in vivo toxicity of a commercial grade boron nitride nanotube mixture

**Vamsi K. Kodali, Jenny R. Roberts, Mohammad Shoeb, Michael G. Wolfarth, Lindsey Bishop, Tracy Eye, Mark Barger, Katherine A. Roach, Sherri Friend, Diane Schwegler-Berry, Bean T. Chen, Aleksandr Stefaniak, Kevin C. Jordan, Roy R. Whitney, Dale W. Porter & Aaron D. Erdely**

**To cite this article:** Vamsi K. Kodali, Jenny R. Roberts, Mohammad Shoeb, Michael G. Wolfarth, Lindsey Bishop, Tracy Eye, Mark Barger, Katherine A. Roach, Sherri Friend, Diane Schwegler-Berry, Bean T. Chen, Aleksandr Stefaniak, Kevin C. Jordan, Roy R. Whitney, Dale W. Porter & Aaron D. Erdely (2017): Acute in vitro and in vivo toxicity of a commercial grade boron nitride nanotube mixture, Nanotoxicology, DOI: 10.1080/17435390.2017.1390177

**To link to this article:** http://dx.doi.org/10.1080/17435390.2017.1390177

View supplementary material

Published online: 02 Nov 2017.

Submit your article to this journal

View related articles

View Crossmark data

Full Terms & Conditions of access and use can be found at
http://www.tandfonline.com/action/journalInformation?journalCode=inan20

**Download by:** [98.239.138.184] **Date:** 02 November 2017, At: 14:18

NANOTOXICOLOGY, 2017
https://doi.org/10.1080/17435390.2017.1390177

ARTICLE

# Acute *in vitro* and *in vivo* toxicity of a commercial grade boron nitride nanotube mixture

Vamsi K. Kodali[a], Jenny R. Roberts[a], Mohammad Shoeb[a], Michael G. Wolfarth[a], Lindsey Bishop[a], Tracy Eye[a], Mark Barger[a], Katherine A. Roach[a], Sherri Friend[a], Diane Schwegler-Berry[a], Bean T. Chen[a], Aleksandr Stefaniak[a], Kevin C. Jordan[b], Roy R. Whitney[b], Dale W. Porter[a] and Aaron D. Erdely[a]

[a]National Institute for Occupational Safety and Health, Morgantown, WV, USA; [b]BNNT LLC, Newport News, VA, USA

**ABSTRACT**

Boron nitride nanotubes (BNNTs) are an emerging engineered nanomaterial attracting significant attention due to superior electrical, chemical and thermal properties. Currently, the toxicity profile of this material is largely unknown. Commercial grade BNNTs are composed of a mixture (BNNT-M) of ~50–60% BNNTs, and ~40–50% impurities of boron and hexagonal boron nitride. We performed acute *in vitro* and *in vivo* studies with commercial grade BNNT-M, dispersed by sonication in vehicle, in comparison to the extensively studied multiwalled carbon nanotube-7 (MWCNT-7). THP-1 wild-type and NLRP3-deficient human monocytic cells were exposed to 0–100 μg/ml and C57BL/6 J male mice were treated with 40 μg of BNNT-M for *in vitro* and *in vivo* studies, respectively. *In vitro*, BNNT-M induced a dose-dependent increase in cytotoxicity and oxidative stress. This was confirmed *in vivo* following acute exposure increase in bronchoalveolar lavage levels of lactate dehydrogenase, pulmonary polymorphonuclear cell influx, loss in mitochondrial membrane potential and augmented levels of 4-hydroxynonenal. Uptake of this material caused lysosomal destabilization, pyroptosis and inflammasome activation, corroborated by an increase in cathepsin B, caspase 1, increased protein levels of IL-1β and IL-18 both *in vitro* and *in vivo*. Attenuation of these effects in NLRP3-deficient THP-1 cells confirmed NLRP3-dependent inflammasome activation by BNNT-M. BNNT-M induced a similar profile of inflammatory pulmonary protein production when compared to MWCNT-7. Functionally, pretreatment with BNNT-M caused suppression in bacterial uptake by THP-1 cells, an effect that was mirrored in challenged alveolar macrophages collected from exposed mice and attenuated with NLRP3 deficiency. Analysis of cytokines secreted by LPS-challenged alveolar macrophages collected after *in vivo* exposure to dispersions of BNNT-M showed a differential macrophage response. The observed results demonstrated acute inflammation and toxicity *in vitro* and *in vivo* following exposure to sonicated BNNT-M was in part due to NLRP3 inflammasome activation.

**ARTICLE HISTORY**
Received 23 May 2017
Revised 1 September 2017
Accepted 3 October 2017

**KEYWORDS**
Boron nitride nanotubes; MWCNT-7; lysosomal damage; NALP3 inflammasome; inflammation; phagocytosis; pyroptosis

## Introduction

For just more than a decade, extensive research has gone into investigating the potential toxicities of engineered nanomaterials (ENMs). The understanding was warranted given that estimates predicted six million workers would be needed in the manufacture of nano-based products and that nanotechnology would have a $3 trillion dollar impact on the global economy by 2020 (NIOSH 2013; Roco, Mirkin, and Hersam 2011). A wide variety of ENMs exist and the possible permutations of each are innumerable. To combat the large numbers of engineered nanomaterials, categorization based on physical and chemical characteristics has been recommended. (Godwin et al. 2015; Kuempel et al. 2012). For example, highly reactive spherical particles, such as some metal oxide nanoparticles, can be distinguished from high aspect ratio particles such as carbon nanotubes. Categorization allows for predictive grouping of associated general mechanisms of toxicity. This is important when assessing safety by design of a known particle or screening for the toxicity of emerging ENMs.

**CONTACT** Aaron Erdely ✉ efi4@cdc.gov NIOSH/HELD/PPRB, 1095 Willowdale Rd, MS-2015, Morgantown, WV 26505-2888, USA

Supplemental data for this article can be accessed here.

This work was authored as part of the Contributor's official duties as an Employee of the United States Government and is therefore a work of the United States Government. In accordance with 17 U.S.C. 105, no copyright protection is available for such works under U.S. Law.

One of the most widely studied categories of engineered nanomaterials are the biopersistent high aspect ratio materials that induce fibrosis. The majority of toxicity studies have been performed on carbon nanotubes (CNTs). CNTs are capable of inducing carcinogenicity, alveolar fibrosis, neuroinflammation and systemic inflammation at certain exposure levels (Erdely et al. 2009; Aragon et al. 2016, 2017; Mercer et al. 2013; Sargent et al. 2014). These findings have led to reviews of general toxicity, adverse outcome pathways (AOPs) highlighting specific mechanisms of disease and a recommended exposure limit. (NIOSH 2013; Oberdörster et al. 2015; Vietti, Lison, and van den Brule 2016; Villeneuve et al. 2014; Labib et al. 2016). These findings formed the foundation for the focused assessment of emerging ENMs with similar physicochemical characteristics.

One such material in the category of newly emerging ENM is the boron nitride nanotube (BNNT). BNNTs are tubes with alternating boron and nitrogen atoms synthesized from boron and nitrogen precursors making it similar in structure to a CNT. BNNTs are manufactured to be less than 100 nm in diameter while being microns in length. Those characteristics classify BNNTs as a high aspect ratio particle. Therefore, based on structural analogy, the potential exists for similar pathology as CNT. BNNTs, like their structural multi-walled CNT (MWCNT) analog, not only have robust mechanical properties but also excellent thermal and chemical properties. They are transparent and with a large band gap (5.5 eV) are electrically insulating, making them a great candidate for high-end engineering applications like lightweight/high-temperature ceramic components, flame-retardant insulations, etc. To date, very few studies have explored the toxicity of BNNTs, and those studies were primarily *in vitro* and descriptive. The results from these previous studies were also conflicting as several of those studies indicated minimal to no toxicity in response to BNNT treatment (Chen et al. 2009; Ciofani et al. 2010; Rocca et al. 2016; Ferreira et al. 2011; Rasel et al. 2015) while another indicated dose- and time-dependent toxicity. (Horvath et al. 2011). It was the suggestion of Horvath et al., that further investigation into the toxicity of BNNTs was warranted especially *in vivo*. (Horvath et al. 2011)

The purpose of the current study was to evaluate mechanistic molecular initiating events occurring due to acute exposure of BNNTs *in vitro* and *in vivo* in a complementary experimental design. Since occupational settings where BNNTs are manufactured represent a potential exposure scenario, we chose a commercially produced BNNT as the primary particle for investigation. Commercially produced BNNT is a mixture (BNNT-M) that consists of 50–60% by mass BNNT, and 40–50% by mass impurities of boron and hexagonal boron nitride. THP-1 human blood monocyte cell line, both wild-type (WT) and NALP3 inflammasome deficient cells, were evaluated for cytotoxicity, inflammation and oxidative stress following BNNT-M treatment. Also, alterations in macrophage response and function following a secondary challenge after BNNT-M treatment were evaluated. The outcomes of the *in vitro* studies were confirmed *in vivo* in mice exposed to BNNT-M by oropharyngeal aspiration. To get a thorough understanding, the toxicity was compared to an extensively studied MWCNT, MWCNT-7. MWCNT-7 was chosen as a reference particle because the mechanisms of toxicity have been described more so than for any other MWCNT.

The study showed BNNT-M-induced oxidative stress and inflammation in part through a NALP3 inflammasome-dependent manner. The results were confirmed *in vivo*. Comparatively, MWCNT-7 conferred greater toxicity on an equal mass basis. THP-1 cells or alveolar macrophages obtained and challenged *ex vivo* following BNNT-M exposure exhibited an altered inflammatory response and reduced capacity to combat a secondary infection. Based on molecular initiating events determined in the current study, further focused BNNT-M AOPs studies based on current MWCNT AOPs may be warranted, including *in vivo* subchronic investigations to determine biopersistence and the potential development of significant histopathological alterations.

## Materials and methods

### *Material characterization, dispersion and endotoxin testing*

The MWCNT used in this study have been extensively characterized previously. (Porter et al. 2010) The average diameter was 49 nm with a length of

3.86 μm (GSD 1.94). The particles were dispersed as previously described by Porter et al. (Porter et al. 2008) in dispersion media (DM) containing mouse serum albumin (0.6 mg/ml final concentration) and 1,2-dipalmitoyl-sn-glycero-3-phosphocholine (DPPC; 10 μg/ml) then diluted 1:1 in DM or cell culture media for dosing. The DM has been shown to be nontoxic itself and to not mask toxicity of particles. BNNT used in this study was provided by a commercial manufacturer of boron nitride nanotubes through a material transfer agreement (MTA) with the coauthors and their research institute. The manufacturer's data sheet specified that the samples had a residual precursor materials (boron, amorphous boron nitride and hexagonal boron nitride). Primary particle size of the BNNTs were described as approximately 5–6 nm × 200 μm length. We have characterized the dimension of the material following preparation and isolation. Material was weighed and suspended in 100% ethanol and sonicated for 5 min in a cup-holder sonicator. Samples were then dried to remove ethanol. At this stage, particles were sized with point count methods. The samples that were delivered to the animals ranged in width of 13–23 nm (likely agglomerating along their length) and in lengths between 0.6–1.6 μm. Agglomerates of material ranged in geometric equivalent diameter by ~0.1–0.3 μm. To eliminate the possibility of endotoxin contamination as a confounder, we tested the stocks of both BNNT-M and MWCNT-7 for endotoxin contamination using a chromogenic limulus amebocyte lysate assay (Genscript ToxinSensor$^{TM}$ Chromogenic LAL Endotoxin Assay Kit, Genscript # L00351, Piscataway, NJ) as per manufacturer's instructions. The endotoxin test was performed at a nanomaterial concentration of 1 μg/μl and the level of endotoxin tested in the ENMs was below 0.1 EU/ml. Dynamic light scattering (DLS) was used to measure agglomerate size distribution and agglomerate charge (zeta potential) using Malvern Zetasizer Nano ZS90 (Worcestershire, UK) equipped with a 633 nm laser at a 90° scattering angle. Particles were prepared in DM at 5 mg/ml and all measurements were performed at a particle concentration of 50 μg/ml in water, PBS and RPMI cell culture media, while maintaining a constant temperature of 25 °C. Samples were equilibrated inside the instrument for two minutes, and five measurements, each consisting of at least five runs, were recorded.

### *Animals, bronchoalveolar lavage, alveolar macrophage (AM) enrichment and culture*

Pathogen-free, male C57BL/6 J mice from Jackson Laboratory (Bar Harbor, ME) were used in this study. All mice housed in the AAALAC International approved NIOSH Animal Facility were provided food and tap water *ad libitum* in ventilated cages in a controlled humidity and temperature environment with a 12-h light/dark cycle. Animal care and use procedures were conducted in accordance with the 'PHS Policy on Humane Care and Use of Laboratory Animals' (NIH 1986) and the 'Guide for the Care and Use of Laboratory Animals' (National Research Council 2011). These procedures were approved by the National Institute for Occupational Safety and Health Institutional Animal Care and Use Committee. Two separate blocks of mice were exposed to DM ($n = 6 \times 2 = 12$), BNNT-M (40 μg/mouse, $n = 6 \times 2 = 12$) or MWCNT-7 (40 μg/mouse, $n = 6 \times 2 = 12$) and sacrificed 24-h post-exposure. Mice were exposed via oropharyngeal aspiration. Briefly, each mouse was placed in a glass jar with a gauze pad moistened with isoflurane (Abbott Laboratories, North Chicago, IL) until slowed breathing was observed. The mouse was then suspended, by its top incisors, on a slanted board in a supine position. The tongue was extended with forceps and the solution was placed by pipette at the back of the throat. The tongue was held extended until the solution was aspirated into the lung and the mouse resumed a regular breathing pattern.

Mice were humanely euthanized with an overdose of sodium pentobarbital (>100 mg/kg, Fort Dodge Animal Health, Fort Dodge, IA). Bronchoalveolar lavage (BAL) was obtained with the trachea cannulated with a blunted 22-gauge needle and, while massaging the thorax, 0.6 ml of cold PBS was slowly instilled into the lung then withdrawn and placed into a 15-ml conical tube. This constituted the first fraction BAL fluid. Two subsequent lavages (1.0 ml/instillate) were collected into a separate tube which represented the second fraction. The BAL fluid was preserved on ice until centrifugation (500 × *g*, 10 min, 4 °C). Aliquots of the first fraction BAL supernatant were used to assess lung injury or frozen at −80 °C for later analysis. The supernatant of the second fraction was discarded. The cell pellets from both fractions were combined for subsequent analysis.

### Cell differentials

For estimating the cell differentials in bronchoalveolar lavage, BAL cells in the lavage fluid were plated onto glass slides using a Cytospin 3 centrifuge (Shandon Life Sciences International, Cheshire, England) set at 800 rpm for 5 min. Slides were stained using Leukostat stain (Fisher Scientific, Pittsburgh, PA) then coverslipped. A minimum of 300 cells/slide consisting of alveolar macrophages/monocytes, lymphocytes or polymorphonuclear cells were identified and manually counted using light microscopy. Slides from shams (DM exposed) animals consisted typically of >99% alveolar macrophages.

### Cell culture

Human peripheral blood monocyte cell line, THP-1 cells, were cultured, differentiated, and primed using procedures described previously by Xia et al. (2013). In brief, human monocyte THP-1 cells (ATCC # TIB 202) were grown in RPMI-1640 media supplemented with 10% fetal bovine serum (FBS), 100 μg/mL penicillin–streptomycin, and 50 μM of beta-mercaptoethanol. NLRP3-deficient (defNLRP3) THP-1 cells were purchased from InvivoGen (San Diego, CA) and grown in RPMI-1640 media supplemented with 10% FBS and 100 μg/ml penicillin–streptomycin and 300 μg/ml Hygromycin. THP-1 cells were differentiated into macrophages by treating them with vitamin D3 at 150 nM overnight and then 5 nM PMA for 12 h. As described previously (Xia et al. 2013), differentiated THP-1 cells were primed to induce the transcription of pro-IL-1β by culturing with 10 ng/ml LPS for 12 h before nanomaterial challenge.

### Cytotoxicity, oxidative stress and high content epifluorescence microscopy

*In vitro*, membrane integrity of the cells after nanomaterial treatment was assessed using CytoTox-One homogenous membrane integrity assay (Promega, Madison, WI). *In vivo*, the cytotoxicity induced by nanomaterials was assessed by measuring LDH in the first acellular fraction of BALF of the mice using a COBAS MIRA Plus autoanalyzer (Roche Diagnostics Systems, Mount Clair, NJ). A dose-response of the oxidative stress induced by BNNT-M was evaluated using Dichloro-dihydrofluorescein diacetate (DCF) using high content microscopy. 10 000 cells were plated on a glass bottom 96-well plate (Greiner Bio-One, Monroe, NC) and after 24 h of nanomaterial exposure, the media were replaced with a cocktail containing Hoechst 33342 (1 μM) and DCF (5 μM). After 30 min of incubation, the 96-well plate was washed three times and imaged using a high content screening epifluorescence microscope Image-Xpress$^{micro}$ (Molecular Devices, Sunnyvale, CA). Images were collected using DAPI and FITC filter/dichroic combinations to image Hoechst 33342 (blue) and DCF (green), respectively, under 10× magnification. The microscopic images were automatically analyzed by Meta-Xpress software (Molecular Devices, Sunnyvale, CA). The percent of cells positive for a DCF cellular response was calculated based on the total cell number (Hoechst 33 342 positive cells). The experiment was performed with six replicates in each group and measurements of 15 000 to 20 000 cells per each replicate. *In vivo*, oxidative stress was qualitatively evaluated by measuring 4-Hydroxynonenal in isolated alveolar macrophages from BAL fluid using anti-4 hydroxynonenal (4-HNE) antibody (ABCAM Inc., Cambridge, MA, ab46545). Alteration in mitochondrial membrane potential (ΔM) was evaluated using JC-1 (Molecular Probes Inc, T3168). JC-1 undergoes a reversible change in fluorescence emission from green to red as mitochondrial membrane potential increases. Cells with high membrane potential promote the formation of dye aggregates and fluoresce red, while cells with low potential contain monomeric JC-1 and fluoresce green. 4-HNE adduct formation and mitochondrial membrane potential was measured in isolated alveolar macrophages from lavage fluid of animals treated with ENMs. The isolated PMNs were re-suspended in PBS, spun down with the Cytospin 3 centrifuge, fixed in 10% formalin, rinsed with PBS, blocked (2% BSA and 0.3% Triton X) for 2 h and incubated with 4-HNE antibodies overnight. The slides were further washed with PBS and incubated with Alexa 488 secondary antibody for 45 min. For JC-1 labeling, cells from cytospins were incubated with JC-1 dye for 15 min and then fixed with 10% formalin. The slides were finally washed in PBS twice and mounted with ProLong Gold.

### *Electron microscopy*

THP-1 macrophages after the exposure period were washed twice with DPBS, fixed with Karnovsky's fixative buffered in 0.1 M sodium cacodylate. Cells from BAL fluid of mice exposed to BNNT-M were collected by centrifugation and were also fixed with Karnovsky's fixative buffered in 0.1 M sodium cacodylate. Cells were then postfixed in 1% osmium tetroxide; stained *en bloc* with 1% tannic acid and 0.5% filtered uranyl acetate; dehydrated with a graded series of ethanols; infiltrated with propylene oxide and LX-112 epon; and embedded in LX-112 epon. Sections were cut at 70 nm, placed on 200 mesh copper grids and stained with 4% uranyl acetate and Reynolds' lead citrate. Images were taken using a JEOL JEM 1400 transmission electron microscope (JEOL USA) with an AMT XR-81 M-B digital camera attachment.

For obtaining electron microscopy image of BNNT-M particulate, bulk BNNT-M particles were initially dispersed in DM. These samples were further vortexed and diluted 1:100 with filtered distilled water. For transmission electron microscopy, one drop of the diluted particle solution was placed on a Formvar-coated 200 mesh copper grid and allowed to dry overnight. For scanning electron microscopy, the same 0.5 ml of the same diluted sample was withdrawn and filtered under vacuum onto a 0.2-micron polycarbonate filter. The filter was then mounted onto an aluminum stub using carbon double-stick tape. The sample was sputter coated with gold–palladium, and imaged using a Hitachi S4800 field-emission scanning electron microscope (Hitachi, Japan).

### *Lysosomal membrane permeabilization*

Quantification of lysosomal membrane permeabilization was performed using acridine orange (AO) staining. Primed and differentiated THP-1 macrophage cells were exposed to 5 µg/ml of the lysosomotropic metachromatic fluorophore and weak base AO (Molecular Probes, OR) for 15 min, then washed and challenged with 25 µg/ml of BNNT-M for 2 h. Cells were washed thrice with warm PBS and increase green fluorescence occurring due to lysosomal membrane permeabilization was quantified using single-cell fluorescence of 10 000 cells measured using BD LSR II flow cytometer (BD Biosciences, San Diego, CA). The fluorescence was quantified using FlowJo (FlowJo LLC, Ashland, OR, USA).

### *Cytokine analysis*

IL-1β and IL-18 production in differentiated and primed THP-1 culture supernatants and mouse BAL fluid was determined using human and mouse IL-1β ELISA kits (R&D Systems, Minneapolis, MN) and IL-18 ELISA kits (MBL international, MA) following the manufacturers recommendation. Multiplex cytokine analysis was performed on BAL fluid and cell supernatants of AMs challenged with and without 1 µg/ml LPS using the Milliplex MAP Mouse Cytokine/Chemokine 32-plex assay (Millipore) on a BioPlex 200 (Bio-Rad Laboratories, Inc., Hercules, CA) and performed by Eve technologies (Eve Technologies, Calgary, Alberta, Canada) . The 32-plex consisted of Eotaxin, G-CSF, GM-CSF, IFNγ, IL-1α, IL-1β, IL-2, IL-3, IL-4, IL-5, IL-6, IL-7, IL-9, IL-10, IL-12 (p40), IL-12 (p70), IL-13, IL-15, IL-17, IP-10, KC, LIF, LIX, MCP-1, M-CSF, MIG, MIP-1α, MIP-1β, MIP-2, RANTES, TNFα and VEGF. The assay sensitivities for these markers ranged from 0.1 to 33.3 pg/mL.

### *Cathepsin B and caspase-1*

After 6 h of nanoparticle exposure, cells were incubated for 30 min at 37 °C with fresh medium containing either fluorescent cathepsin B substrate Magic Red$^{TM}$ (MR-(RR)$_2$) or with fluorochrome inhibitor of caspase-1 (FAM-YVAD-FMK) according to manufacturer's recommendations (Immunochemistry Technologies LLC, Bloomington, MN). Cathepsin B or Caspase-1 activity inside the cells were quantified using single cell fluorescence of 10 000 cells measured using BD LSR II flow cytometer (BD Biosciences, San Diego, CA) and analyzed using FlowJo (FlowJo LLC, Ashland, OR, USA). For microscopy analysis, cells were grown on glass slides and after exposure to nanomaterials and the fluorescent indicator for the required experimental time, cells were fixed using 3% paraformaldehyde, washed and mounted using ProLong Gold (Invitrogen, Carlsbad, CA). Confocal images were obtained using a Zeiss LSM 710 upright confocal microscope (Carl Zeiss Microscopy, LLC., Thornwood, NY) with a 40 × water immersion objective.

### *Phagocytosis and LPS challenge functional assays*

*In vitro*, differentiated and primed THP-1 cells were exposed to various concentrations of BNNT-M (0–100 μg/ml) for 24 h and were further challenged with fresh medium containing *Escherichia coli* GFP (ATCC # 25922GFP) at multiplicity of infection (MOI) of 1:25. In order for the bacteria to reach the cells at the bottom of the well, the plate containing the cells and bacteria was centrifuged at 1000 rpm for 10 min before placing them in an incubator at 37 °C. After 2 h of challenge, the cells were washed with PBS, harvested by trypsinization and scraping, centrifuged at 1000 *g* for 5 min and resuspended in PBS. The cell-associated bacteria was quantified using a BD LSR II flow cytometer (BD Biosciences, San Diego, CA). All experiments were performed using triplicate samples and at least 10 000 cells were analyzed per treatment. The mean fluorescence was determined using FlowJo (FlowJo LLC, Ashland, Oregon). For *ex vivo* analysis of bacterial uptake by AM after BNNT-M pretreatment, mice ($n = 6$ for each group) were exposed to either DM or BNNT-M (40 μg). After 24 h, AM from BAL fluid were collected and enriched by adhesion to tissue culture plates for 2 h in fresh Eagle's minimum essential medium (Lonza BioWhittaker, Walkersville, MD). Bacterial challenge, collection and quantification was done as explained in the *in vitro* section earlier. The enriched AMs were also challenged with 1 μg/ml of LPS for 12 h and the cytokines secreted were measured from the supernatants using Milliplex MAP Mouse Cytokine/Chemokine 32-plex assay described earlier in the materials and methods.

### *Statistical methods*

All data are presented as mean with standard deviation or standard error as mentioned in the legend. Analyses were performed using Sigma Plot Software (Systat Software, Inc). Treatments were compared by a one-way analysis of variance (ANOVA) followed by a *post hoc* Student's *t*-test. Differences were considered statistically significant at $p < .05$.

## Results and discussion

### *Characterizing the BNNT suspension*

The high-temperature high-pressure process (Smith et al. 2009) by which BNNTs are manufactured in large-scale results in a commercial-grade mixture containing BNNTs and byproducts. The byproducts, which consist of 40–50% by mass of the BNNT-M, include boron and hexagonal boron nitride. The BNNT-M used in the current study were manufactured to have primary BNNTs which were 5 nm in diameter and up to 200 μm in length and were provided by BNNT, LLC (VA). Samples were sonicated in ethanol to disperse the material, dried and resuspended in dispersion media consisting of serum albumin (0.6 mg/ml) and 1,2-dipalmitoyl-sn-glycero-3-phosphocholine (DPPC; 0.01 mg/ml) prepared in United States Pharmacopeia (USP) grade-phosphate buffered saline (PBS) without calcium and magnesium. The dispersion procedure resulted in a diameter of 13–23 nm which indicated agglomeration of primary BNNTs and a length of 0.6–1.6 μm as assessed by transmission electron microscopy (Figure 1(A1)). Dispersion of BNNTs, a constraint for commercialization, was challenging and resulted in a reduction of the intended length. Methods are being developed and tested to preserve the length of BNNTs for testing given the known adverse potential of high aspect ratio materials. The MWCNT used for comparison in this study, MWCNT-7, has been extensively characterized (Porter et al. 2010; Chen et al. 2012) with an average diameter of 49 nm with a length of 3.86 μm (geometric standard deviation =1.94) and a purity of >99% carbon. The specific surface area of the BNNT-M was 183 ± 3 $m^2/g$ and a density of 0.03 $g/cm^3$. Both BNNT-M and MWCNT-7 had endotoxin lower than the detection limit (<0.01 EU/ml). There were minimal discrepancies between BNNT-M and MWCNT-7 in terms of zeta potential and hydrodynamic diameter in varying biological suspensions (Figure 1(A2)).

### *Cytotoxicity and oxidative stress*

In order to evaluate the biological effects of BNNT-M, we first measured the toxicity in THP-1 cells over a range of doses (0–100 μg/ml or 0–31.25 $\mu g/cm^2$) for 24 h and verified response in C57BL/6 J mice dosed with 40 μg BNNT-M and assessed 24-h post-exposure. MWCNT-7 served as a comparative control. There was a dose-dependent increase in lactate dehydrogenase (LDH) release in THP-1 cells exposed to BNNT-M or MWCNT-7 (Figure 2(A)). At higher exposure conditions (>25 μg/ml or >7.8 $\mu g/cm^2$),

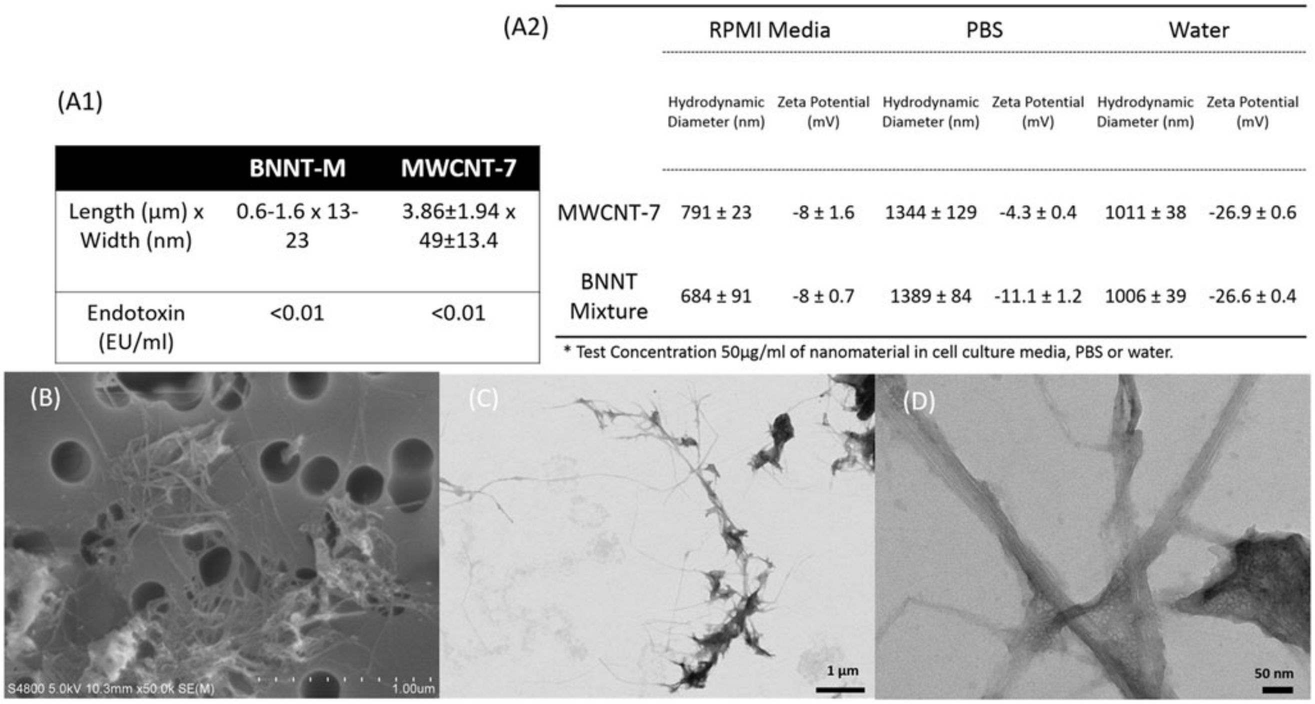

(A1)

| | BNNT-M | MWCNT-7 |
|---|---|---|
| Length (µm) x Width (nm) | 0.6-1.6 x 13-23 | 3.86±1.94 x 49±13.4 |
| Endotoxin (EU/ml) | <0.01 | <0.01 |

(A2)

| | RPMI Media | | PBS | | Water | |
|---|---|---|---|---|---|---|
| | Hydrodynamic Diameter (nm) | Zeta Potential (mV) | Hydrodynamic Diameter (nm) | Zeta Potential (mV) | Hydrodynamic Diameter (nm) | Zeta Potential (mV) |
| MWCNT-7 | 791 ± 23 | -8 ± 1.6 | 1344 ± 129 | -4.3 ± 0.4 | 1011 ± 38 | -26.9 ± 0.6 |
| BNNT Mixture | 684 ± 91 | -8 ± 0.7 | 1389 ± 84 | -11.1 ± 1.2 | 1006 ± 39 | -26.6 ± 0.4 |

* Test Concentration 50µg/ml of nanomaterial in cell culture media, PBS or water.

**Figure 1.** Physicochemical characterization of BNNT-M and MWCNT-7. Table (A1) shows physical characteristics of BNNT-M and MWCNT-7. Table (A2) shows agglomerate size and charge of BNNT-M and MWCNT-7 in various media. Representative SEM (B) and TEM (C) image of dispersed BNNT-M in DM. High resolution TEM image shows structure of BNNT-M at high magnification (D). The images reveal that the major components of the dispersion were BNNTs with some byproducts in the agglomerates.

MWCNT-7 induced significantly more cytotoxicity than BNNT-M, although these effects occurred in the nonlinear phase of the response. There was no statistically significant difference in cytotoxicity between BNNT-M and MWCNT-7 at lower exposure conditions (<25 µg/ml or <7.8 µg/cm$^2$). *In vivo,* induced cytotoxicity was assessed by measuring LDH in bronchoalveolar lavage fluid (BALF) of C57BL/6 J mice exposed to dispersion media (DM), BNNT-M (40 µg), or MWCNT-7 (40 µg) and assessed 24 h postexposure (Figure 2(B)). BNNT-M caused ∼2-fold change while MWCNT-7 caused ∼2.5-fold change in BALF LDH levels. The LDH values for MWCNT-7 were consistent with previous exposures (Porter et al. 2010). In agreement with our *in vitro* results, *in vivo* exposure to BNNT-M induced slightly lower toxicity compared to MWCNT-7 at an equal mass dose. These results contradict the few *in vitro* BNNT cytotoxicity studies performed using complementary assays in various cell types. Studies from Chen et al., Ciofani et al., and others (Chen et al. 2009; Ciofani et al. 2010; Rocca et al. 2016; Ferreira et al. 2011) showed no toxicity due to BNNT. Horvath et al. (Horvath et al. 2011) showed BNNT to be toxic, and the cytotoxicity induced by BNNT was significantly more than MWCNT in all cell lines tested. Our results indicate that BNNT-M induced moderate toxicity in line with Horvath et al. (Horvath et al. 2011), but the toxicity was less than what was induced by MWCNT-7. These discrepancies may be arising due to various BNNT and MWCNT physical forms/mixtures, coatings, dispersion procedures, cell types and toxicological assays employed in these *in vitro* studies. The BNNT used by Horvath et al., were 50 nm in diameter on average (5 nm as-produced with 13–23 nm aggregates tested in this study) and the MWCNT were 20 nm (49 nm tested in this study). Therefore, if diameter was considered as the primary contributing factor to toxicity rather than the specific tested particle, the results of two studies would be complementary. The *in vivo* BNNT-M toxicity data in the present study cannot be directly compared to previous studies, as it is the first study to evaluate the *in vivo* pulmonary toxicity induced by BNNT-M exposure.

Oxidative stress has been proposed as a leading mechanism of toxicity and a nanomaterial's ability to generate oxidative stress has been suggested as a predictor of its toxicity potential (Kodali and Thrall 2015; Zhang et al. 2012). *In vitro*, reactive oxygen

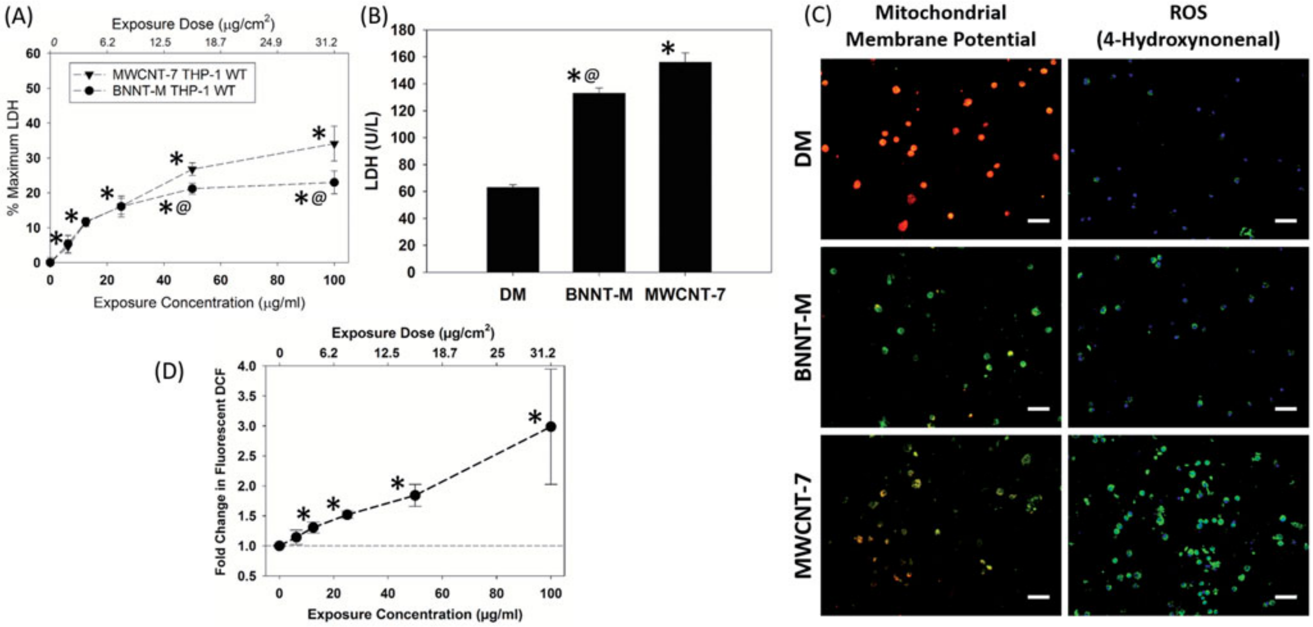

**Figure 2.** Toxicity and oxidative stress induced by BNNT-M with comparison to MWCNT-7. (A) Dose response of cytotoxicity induced by BNNT-M and MWCNT-7 in THP-1 cells using LDH assay. Percent maximum LDH release is LDH release relative to total cell lysis (100% cell death). (B) Comparison of LDH values in BALF from C57BL/6 mice exposed to DM, BNNT-M (40 μg) or MWCNT-7 (40 μg). (C) Oxidative stress induced *in vivo* was qualitatively evaluated by measuring lipid peroxidation (4-hydroxynonenal) and change in mitochondrial membrane potential (JC-1). Images are composites showing green dye aggregates indicating high mitochondrial membrane potential or unhealthy cells and red monomers indicating low mitochondrial membrane potential or healthy cells. Nucleus was supravitally stained with 1 μg/mL Hoechst 33342 for 10 min. The scale bar denotes 50 μm (D) BNNT-M exposure in THP-1 cells increases accumulation of ROS in a dose-dependent manner, as measured by DCF-DA fluorescence. *denotes statistical significance from DM-exposed animals (*in vivo*) or untreated cells (*in vitro*). @ denotes statistical significance ($p < 0.05$) of BNNT-M-exposed animals (*in vivo*) or cells (*in vitro*) from equal exposure concentration of MWCNT-7-exposed animals (*in vivo*) or cells (*in vitro*).

species (ROS) generated in THP-1 cells due to BNNT-M exposure was measured using a fluorometric assay that utilizes intracellular oxidation of 2,7-dichlorohydrofluoroscein diacetate (DCF) and quantified using high content microscopy. BNNT-M exposure in THP-1 cells for 24 h caused a linear dose-dependent increase in DCF fluorescence, reaching significance from control cells at ≥12.5 μg/ml or ≥3.9 μg/cm² (Figure 2(D)). The oxidative potential of BNNT-M was confirmed *in vivo* by examining 4-hydroxynonenal (4-HNE), a stable by-product of lipid peroxidation and loss of mitochondrial membrane potential (ΔM) in alveolar macrophages obtained from mice 24-h post-exposure to 40 μg BNNT-M or MWCNT-7 (Figure 2(C)). Increased 4-HNE (green fluorescence) was observed in alveolar macrophages from MWCNT-7 exposed mice compared to vehicle exposed mice. Fluorescence from 4-HNE increased in alveolar macrophages from BNNT-M-exposed mice compared to vehicle exposed mice but appeared qualitatively less when compared to MWCNT-7 exposed mice. Similar to 4-HNE, a decreased mitochondrial membrane potential, as shown by increased green fluorescence (depolarized or monomeric form) and decreased red fluorescence (polarized or aggregate form) was observed in alveolar macrophages collected from MWCNT-7 and BNNT-M exposed mice. There was no mitochondrial membrane potential change in alveolar macrophages collected from DM exposed mice. Several mechanistic studies provide insight into ROS generation (Dong and Ma 2015; Shvedova et al. 2012) and mitochondrial dysfunction (Nymark et al. 2015) due to CNT exposure. These studies have attributed the ROS generation capacity of CNT to physicochemical properties, surface coatings or the presence of impurities like transition metals. (Johnston et al. 2010; Ge et al. 2012; Tsuruoka, Cassee, and Castranova 2013a; Jiang et al. 2013; Hamilton et al. 2013; Tsuruoka et al. 2013b) In order for BNNTs to achieve full industrial potential and rapid commercialization, extensive mechanistic toxicity studies that delineate the source of ROS, like those performed on MWCNT, are warranted. Nevertheless, in the current study, the

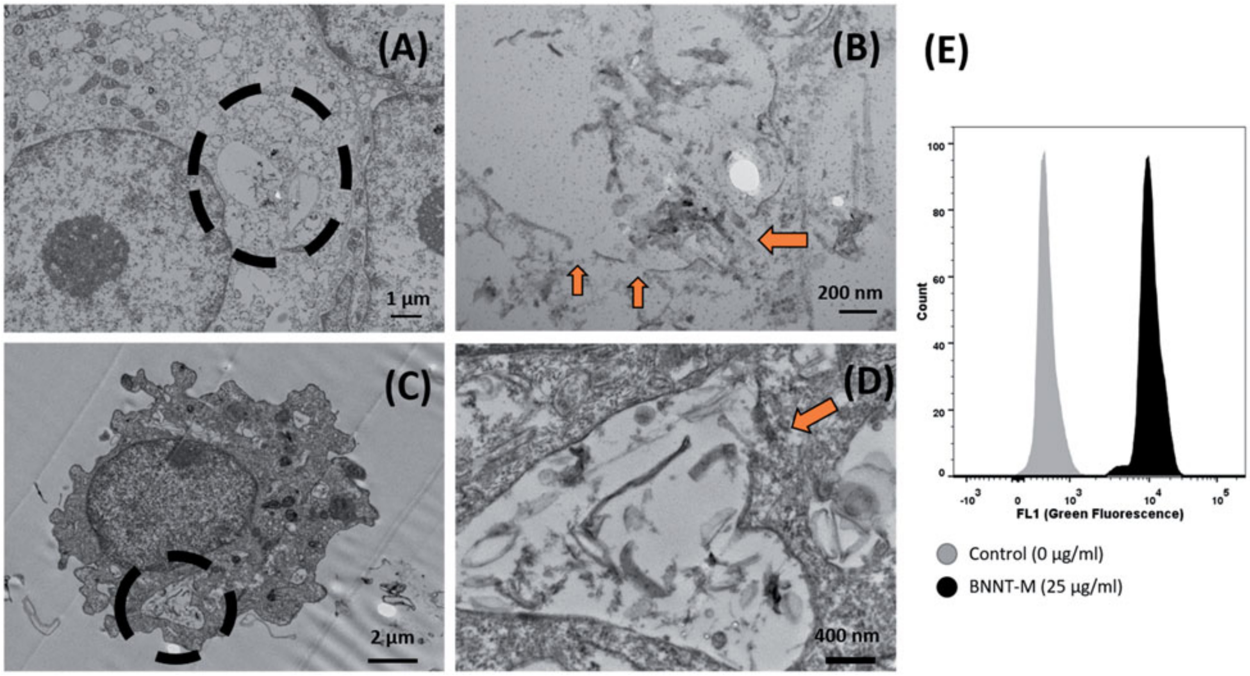

**Figure 3.** Ultrastructural evidence confirming uptake and lysosomal rupture *in vitro* and *in vivo*. (A) TEM image of a differentiated THP-1 macrophage exposed to 25 μg/ml (7.79 μg/cm$^2$) of BNNT-M for 6 h. (B) High magnification image of the circled portion from figure (A) showing a ruptured lysosome (ruptured portion depicted with arrows). Alveolar macrophage from BALF of C57BL/6 mice exposed to BNNT-M (40 μg) for 24 h (C). (D) High magnification image of the circled portion from figure (C) showing a ruptured lysosome (ruptured portion highlighted with arrows). (E) Pretreatment with acridine orange followed by challenge with BNNT-M showed ~20-fold increase in green fluorescence suggesting lysosomal membrane permeabilization.

correlation between ROS and cytotoxicity trends from *in vitro* and *in vivo* BNNT-M exposure suggests a potential ROS-dependent mechanism related to observed cytotoxicity.

### *Lysosomal damage*

In order to directly visualize the effect of BNNT-M on cells *in vitro* and *in vivo*, high magnification ultrastructural images of the cells using transmission electron microscopy (TEM) were taken. Figure 3(A) is a high magnification micrograph of a THP-1 macrophage exposed to 25 μg/ml BNNT-M for 6 h and Figure 3(C) is an alveolar macrophage collected from C57BL/6 J mice exposed to 40 μg of BNNT-M. The images confirm that BNNTs were internalized in both THP-1 and alveolar macrophages. The internalized BNNT-M were in organized vesicles, likely phagosomal–lysosomal vesicles. Figures 3(B,D) are high magnification images of the circled portions in Figure 3(A,C) showing vesicles with BNNT-M. The orange arrows in Figures 3(B,D) point to ruptures in the vesicle membrane. In addition to TEM, acridine orange staining was used to evaluate lysosomal membrane permeabilization. Acridine orange, when in lysosomes is protonated and emits an orange red fluorescence, when the lysosomes are damaged and permeabilized the pH turns neutral turning it to green. The increase in green fluorescence due to lysosomal membrane damage was quantified using flow cytometry. Figure 3(E) represents a histogram of green fluorescence in THP-1 control cells and cells challenged with 25 μg/ml of BNNT-M for 2 h. There was ~20-fold increase in green fluorescence when cells were exposed to BNNT-M suggesting BNNT-M exposure-induced lysosomal damage. In agreement with our BNNT-M exposure results, previous studies delineating mechanisms of nanoparticle-mediated toxicity correlated lysosomal injury to increased cytotoxicity, ROS generation, and mitochondrial dysfunction. (Stern, Adiseshaiah, and Crist 2012; Sun et al. 2015, 2013)

### NLRP3 inflammasome activation and pyroptosis

Lysosome rupture leads to a release of components like cathepsin B into the cytoplasm. Cathepsin B is

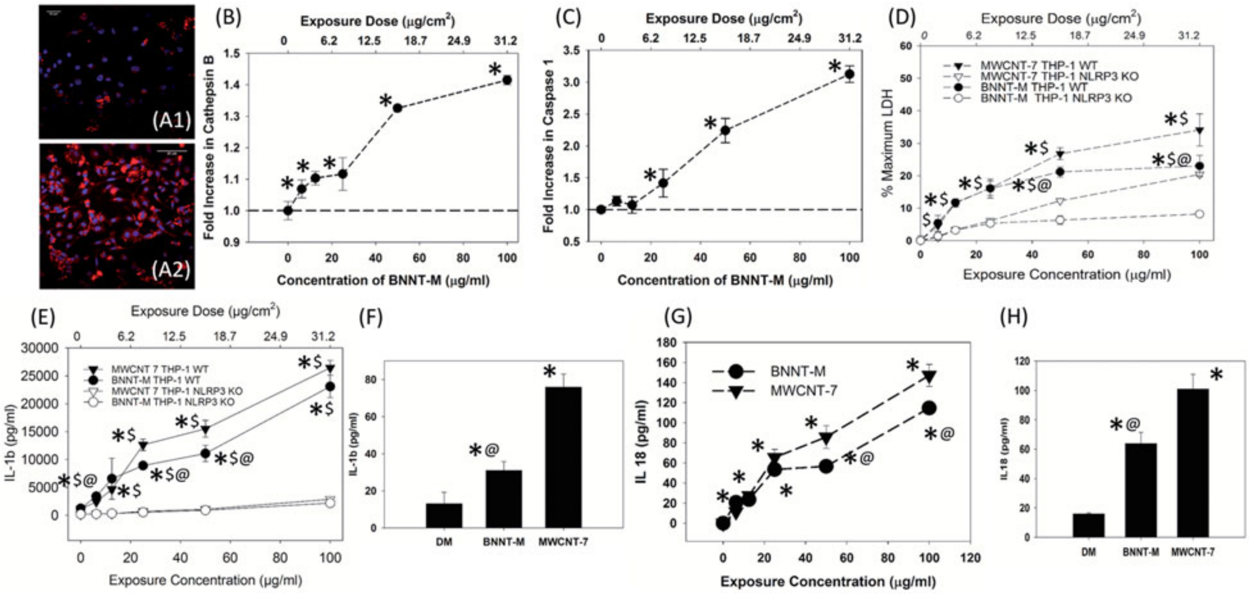

**Figure 4.** BNNT-M caused pyroptosis and induced inflammation *in vitro* and *in vivo*. Confocal images of THP-1 cells without (A1) and with 25 µg/ml (A2) BNNT-M exposure showed increased distribution of active cathepsin B (labeled with Magic Red$^{TM}$). The nucleus was labeled with DAPI. (B) Flow cytometry quantification of cathepsin B activity in THP-1 cells revealed a correlation between dose of BNNT-M exposure and cathepsin B activity in the cells. (C) Similar to cathepsin B activity, a dose-dependent increase in caspase-1 in THP-1 cells exposed to BNNT-M for 6 h was measured. Caspase-1 was detected using FAM FLICA and quantified using flow cytometry. (D) Exposure to MWCNT-7 or BNNT-M in THP-1 WT cells for 24 h induced a dose-dependent increase in cytotoxicity. This toxicity was significantly attenuated with NLRP3 deficiency, suggesting NLRP3-mediated pyroptosis. (E) *In vitro* production of IL-1β by differentiated and primed THP-1 WT and NLRP3-deficient cells. There was a dose-dependent augmentation of IL-1β production in THP-1 WT macrophages with both MWCNT-7 and BNNT-M exposure. IL-1β production was nullified in NLRP3-deficient THP-1 macrophages. (F) IL-1β ELISA of BALF from C57BL/6 mice exposed to BNNT-M or MWCNT-7 (40 µg or ∼0.08 µg/cm$^2$) for 24 h confirms IL-1β release after exposure. (G) *In vitro* production of IL-18 by differentiated and primed THP-1 WT challenged with BNNT-M or MWCNT-7. (H) IL-18 ELISA of BALF from C57BL/6 mice exposed to BNNT-M or MWCNT-7 (40 µg). Taken together, the data suggested BNNT-M induced NLRP3 inflammasome dependent pyroptosis. *denotes statistical significance ($p < 0.05$) from DM exposed animals (*in vivo*) or untreated cells (*In vitro*). @ denotes statistical significance ($p < 0.05$) of BNNT-M-exposed animals (*in vivo*) or cells (*in vitro*) from equal exposure concentration of MWCNT-7-exposed animals (*in vivo*) or cells (*in vitro*). $^\$$denotes statistical significance of THP-1 WT-exposed cells from equal mass exposed THP-1 NLRP3-deficient cells.

considered to be an upstream signal that can activate assembly of a large (700 kDa) multiprotein complex called NLRP3 inflammasome (cryopyrin). THP-1 cells were incubated with Magic Red$^{TM}$ reagent, which produces a fluorescent red product in the presence of active cathepsin B, and exposed to DM (Figure 4(A1)) or BNNT-M (Figure 4(A2)). Confocal images confirm increased active cathepsin B. Flow cytometry quantification of Magic Red demonstrated a dose-dependent increase in cathepsin B with BNNT-M exposure (Figure 4(B)). Even the lowest exposure concentration of 1.95 µg/cm$^2$ caused a statistically significant increase in cathepsin B activity compared to control cells. Our study was primarily designed to examine acute toxicity as an initial screen and, as such, the exposure conditions and time scale were limited. The elevated levels of cathepsin B observed acutely may be transient and subside with time. Even so, the elevated cathepsin B levels warrant dose–response subchronic BNNT-M exposure studies that can evaluate potential adverse health outcomes. Cathepsin B release and subsequent NLRP3 inflammasome activation is known to trigger casapase-1 induction. Flow cytometry quantification of active caspase 1 induced by BNNT-M exposure measured using the fluorescent inhibitor probe FAM-YVAD-FMK showed a dose-dependent increase in caspase 1 with 6 h of BNNT-M treatment (Figure 4(C)). The increase was statistically significant in comparison to control cells with no treatment from a BNNT-M dose ≥7.8 µg/cm$^2$. Caspase 1 is a cysteine-rich protease that is known to cleave key cellular substrates leading to programed cell death. The caspase 1-dependent cell death mechanism is known as pyroptosis (Miao, Rajan, and Aderem 2011). In order to verify NLRP3 dependency in BNNT-M induced inflammasome activation and pyroptosis, studies were performed in THP-1 cells with NLRP3 deficiency. This cell model has been previously used to verify NLRP3 inflammasome dependency for toxicity induced by MWCNT exposure (Sun et al. 2015). At the same exposure conditions, the cytotoxicity induced by MWCNT-7 or BNNT-M (Figure 2(A)) was markedly attenuated in THP-1 NLRP3-deficient cells (Figure 4(D)). The reduced cytotoxicity suggests that NLRP3 was involved in toxicity induced by both MWCNT-7 and BNNT-M. Together the data so far suggests, *in vitro,* BNNT-M exposure results in pyroptosis. Active caspase-1 released due to NLRP3 inflammasome activation is known to cleave the inactive cytoplasmic precursor pro-IL1β converting it into a bioactive and mature IL1β. Previous studies comparing BALF IL-1β levels induced due to exposure of high aspect ratio particles in NLRP3 knockout and wild-type mice showed severe abrogation in IL-1β levels in NLRP3 knockout mice (Dostert et al. 2008; Cassel et al. 2008). To further confirm NLRP3 inflammasome activation due to BNNT-M exposure, a comparison of dose-dependent changes in IL-1β levels in THP-1 WT and NLRP3-deficient cells exposed to BNNT-M or MWCNT-7 for 24 h (Figure 4E) was performed. In wild-type cells, a dose-dependent increase in IL-1β levels with both BNNT-M and MWCNT-7 was measured. MWCNT-7 treatment induced a small increase in IL-1β levels as compared to BNNT-M from a dose $\geq$7.8 μg/cm$^2$. At doses $\leq$7.8 μg/cm$^2$, there was no difference in the amount of IL-1β induced due to BNNT-M or MWCNT-7. The dose-dependent increase in IL-1β production was negated in NLRP3-deficient cells confirming once again the involvement of NLRP3 in BNNT-M-induced inflammasome activation and pyroptosis. To validate this *in vivo,* BAL fluid IL-1β levels were measured in mice exposed to either BNNT (40 μg), MWCNT-7 (40 μg) or DM 24-h postexposure. Although not as dramatic of a difference as in the *in vitro* model, a statistically significant increase was measured in BALF IL-1β of mice exposed to BNNT-M or MWCNT-7 compared with control mice exposed to DM. It is worth noting that BNNT-M induced ∼2.5-fold lower IL-1β than MWCNT-7 *in vivo*. Apart from IL-1β, it is known that inflammasome activation leads to proteolytic cleavage of pro-IL-18 into mature IL-18. As an additional confirmation of inflammasome activation, IL-18 was measured in supernatants of primed and differentiated THP-1 macrophages challenged with MWCNT-7 or BNNT-M at various doses for 24 h and in BALF of mice exposed to 40 μg of DM, BNNT-M or MWCNT-7 (Figure 4(G,H)). *In vitro* there was a significant surge in IL-18 production with even the lowest concentration (i.e. 6.25 μg/ml) of either BNNT-M or MWCNT-7 compared to control cells. *In vivo* both MWCNT-7 and BNNT-M caused a significant increase in IL-18 compared to mice exposed to DM. As with IL-1β, cathepsin B and caspase 1, both *in vivo* and at higher doses *in vitro*, MWCNT-7 induced a greater level of IL-18 compared to equal mass of BNNT-M. Together this data suggests exposure to BNNT-M caused NLRP3 inflammasome activation, albeit to a lower extent compared to the morphologically similar counterpart, MWCNT-7.

### Inflammation induced by BNNT exposure

BALF collected from lungs exposed to various occupational and environmental toxins has a signature of inflammatory cell influx and elevated proteins/cytokines that reflects the injury status and inflammatory state. We evaluated the inflammatory response induced by BNNT-M exposure by measuring 32 secreted proteins/cytokines and accumulation of inflammatory cells in BALF 24 h post-exposure to BNNT-M (40 μg), MWCNT-7 (40 μg), or DM. Polymorphonuclear cell influx is a hallmark of inflammation and tissue injury. Compared to DM exposed mice, a significant increase in percent of BALF neutrophil and eosinophils in mice exposed to both MWCNT-7 and BNNT-M (Figure 5(A)) was measured. The early phase of inflammatory cell influx is exacerbated via various cytokines and chemokines resulting in a multifaceted inflammatory response. The cytokines measured in the BALF provided a partial analysis of the innate immune response induced by BNNT-M. The radar chart in Figure 5(B) depicts cytokines involved in mediating cellular influx and plotted as log 10-fold change to levels measured from BALF of mice exposed to DM (black dots). The trend in cell influx (Figure 5(A)) was mirrored in the cytokine cell influx radar chart (Figure 5(B)). For example, inductions of the human IL-8 homologs, KC and MIP-2, confer to the

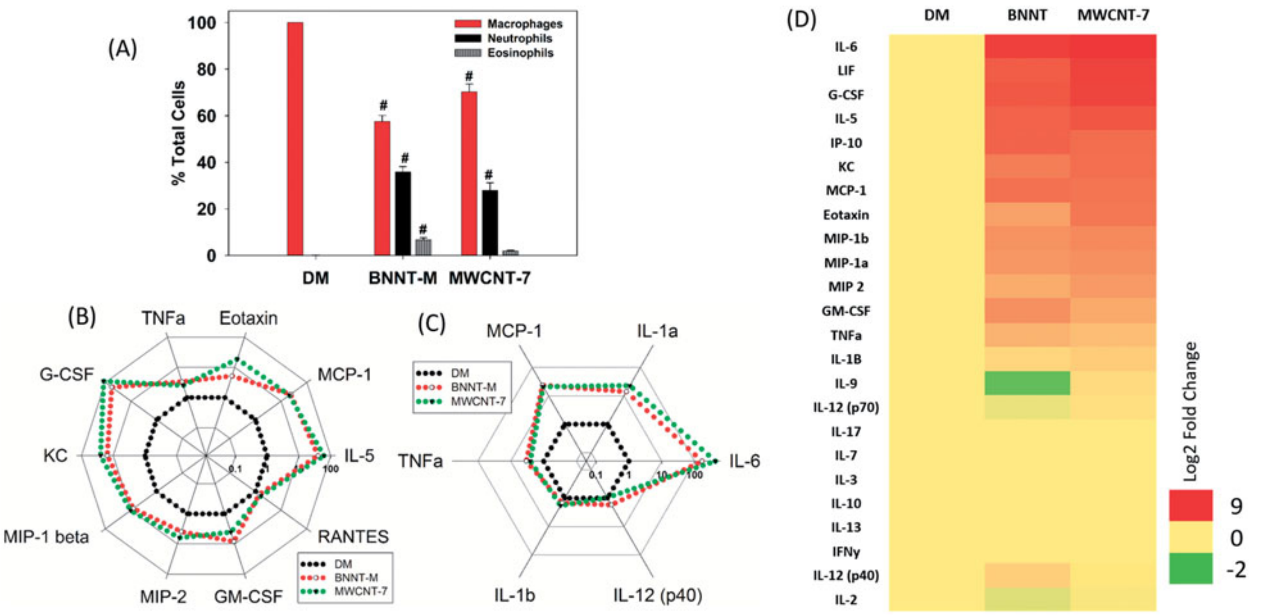

**Figure 5.** Immunotoxicty and inflammatory potential of BNNT-M. (A) Percent (%) Total cells, a measure of pulmonary inflammation in BALF samples 24 h after exposure to DM, BNNT-M (40 µg) or MWCNT-7 (40 µg). Data were expressed as percent (%) Total cells from a total of 300 cells counted slides from cytospins. (B) Multivariant radar chart depicting cytokines responsible for PMN influx measured in BALF samples represented as log 2-fold change from DM exposed values. The cytokines responsible for PMN influx from BNNT-M and MWCNT-7 exposed animals have a similar profile and are in line with the trend observed in Figure 5 (A). (C) Chart depicting pro-inflammatory cytokines in BALF from mice exposed to DM, BNNT-M or MWCNT-7. Based on the cytokines measured, the pro-inflammatory signature induced by MWCNT-7 and BNNT-M was similar. (D) 32 cytokine/chemokines in BALF of mice exposed to DM, MWCNT-7 or BNNT-M (40 µg or ~0.08 µg/cm$^2$) 24 h after exposure. Each data point are an average of BALF from six mice. The heat map represents log 2-fold change with respect to DM exposed mice and segregated into three groups of cytokines expressed in acute, acute and subchronic and subchronic. Across the board, the cytokine profile of BNNT-M was similar to the profile of BALF from MWCNT-7. Albeit similar profile, the absolute amount of inflammatory cytokines induced by BNNT-M exposure was lower than what was induced by MWCNT-7 exposure. Absolute values, fold changes and statistical significance of the cytokine data is available in the attached supplemental information. #denotes statistically significant change ($p < 0.05$) in inflammatory cell influx from DM control.

neutrophil influx, and eotaxin and IL-5 are representative of the eosinophil recruitment. Exposure to MWCNT-7 (green dots) or BNNT-M (red dots) induced a relatively similar profile for cytokines involved in cellular influx. Pyroptosis, or caspase 1-dependent cell death due to NLRP3 inflammasome activation, is inherently pro-inflammatory (Bergsbaken, Fink, and Cookson 2009) Active caspase-1 is known to bind and induce secretion of several pro-inflammatory cytokines including, IL-1β, IL-1α, IL-18, TNFα and IL-6. (Bergsbaken, Fink, and Cookson 2009) Figure 5(C) is a radar chart representing pro-inflammatory cytokines in BAL fluid of mice exposed to MWCNT-7 or BNNT-M plotted as log 10-fold change from cytokines from mice exposed to DM. In agreement with our earlier results, confirming both MWCNT-7 and BNNT-M induced pyroptosis due to NLRP3 inflammasome activation, there was an increase in all the pro-inflammatory cytokines measured following MWCNT-7 or BNNT-M exposure compared to DM (Figure 5(C)). There was a similar pro-inflammatory cytokine profile with MWCNT-7 or BNNT-M exposure. Figure 5(D) is a heat map representing all the cytokines measured. The cytokine/chemokines from BALF of mice exposed to MWCNT-7 or BNNT-M is presented as log 2-fold change from cytokine/chemokines of DM exposed mice. Most of the cytokines that were found elevated were slightly less pronounced with BNNT-M exposure than MWCNT-7 exposure. Although no studies exist for comparing the pulmonary inflammatory response of the BNNT-M *in vivo* exposure, previous studies with MWCNT-7 showed similar acute pulmonary inflammatory profile (Porter et al. 2010, 2012; Oberdörster et al. 2015). The unmodified 32 cytokine/chemokine concentration data, fold change and statistical significance from BALF of mice exposed to DM, MWCNT-7 or BNNT-M have been made available in the supplemental information.

### *Functional changes caused by BNNT exposure*

Epidemiology studies showed exposure to particulates from air pollution caused an increase in hospital admissions for respiratory infectious disease (Schwartz, Dockery, and Neas 1996; Pope 2000). Immune dysfunction due to particle exposure has been hypothesized as a probable cause for this increase in respiratory infections (Zeidler-Erdely, Erdely, and Antonini 2012) Nanomaterial exposure was shown to cause a similar dysregulation in macrophage function (Kodali et al. 2013; Duan et al. 2015). It is also known that NLRP3 inflammasome activation orchestrates multiple innate and adaptive immune responses in infection and auto-inflammatory disorders (Guo, Callaway, and Ting 2015). As such, we evaluated BNNT-M exposure to modulate macrophage function and its ability to respond to subsequent infections. Differentiated THP-1 WT and NLRP3 deficient macrophages were treated with a wide dose range (0–100 μg/ml or 0–25 μg/cm$^2$) of BNNT-M for 24 h and then challenged with green fluorescent protein Escherichia coli (GFP *E.coli*) for 2 h at a multiplicity of infection (MOI) of 25 (Figure 6(A)). GFP *E. coli* uptake by the macrophages was quantified using flow cytometry. With increasing concentration of BNNT-M treatment, phagocytic capacity in THP-1 WT cells decreased. Even the lowest dose of BNNT-M tested, 1.6 μg/cm$^2$, had a statistically significant effect on uptake of bacteria. Removal of NLRP3 protected the macrophage and allowed them to retain their phagocytic capacity until doses of 6.3 μg/cm$^2$ or 25 μg/ml. Even at the higher concentrations tested, ≥6.3 μg/cm$^2$ or ≥25 μg/ml, NLRP3 deficiency enabled the macrophages to maintain phagocytic efficiency much better than WT macrophages. This clearly showed that NLRP3 was involved in the regulation of BNNT-M-induced dysregulation of the macrophage innate immune response. The BNNT-M-induced reduction in phagocytic capacity was further confirmed *ex-vivo*. C57BL/6 mice were exposed to BNNT-M or DM at 40 μg/mouse and the alveolar macrophages obtained from BALF collected 24 h post-exposure were isolated and enriched by adhesion to tissue culture plates for 2 h. The alveolar macrophages, which had already been exposed to BNNT-M or DM *in vivo*, were further challenged with GFP *E.coli* (MOI 25) *ex-vivo* for 2 h, and the uptake of the bacteria was quantified using flow cytometry. At the single dose tested, we saw a 20% decrease in phagocytic capacity of alveolar macrophages from BNNT-M compared to DM exposed mice, further confirming our *in vitro* dose-response data. This decrease in macrophage innate function suggests reprograming in macrophage phenotype. In the current work, GFP E. *coli* was used as a model infectious bacterial agent for assessing pulmonary innate immune function using a spin infection model. Challenge with pulmonary bacterial infectious agents like H. *influenza*, S. *pneumonia* or P. *aeruginosa* etc. as well as a passive infection model may provide further clarity regarding the mechanism and kinetics of impaired pulmonary macrophage phagocytic capacity. To evaluate how pre-exposure to BNNT-M caused changes in the ability of macrophages to respond to a secondary inflammatory insult, we challenged alveolar macrophages from mice exposed to BNNT-M or DM with lipopolysaccharide (LPS), an outer membrane component of gram negative bacteria which is known to induce a strong inflammatory response. By measuring the cytokines after the secondary inflammatory insult of LPS, the intent was to elucidate a snapshot of the modified secondary immunotoxicity responses induced by BNNT-M exposure. Figure 6(C) shows log 2-fold change of cytokines secreted by alveolar macrophages collected 24-h postexposure from mice exposed to BNNT-M or DM and subsequently challenged *ex-vivo* with LPS for 12 h. In general, there was no change in the profile of alveolar macrophages from BNNT-M or DM-treated mice without LPS stimulation (data with absolute values of cytokines in pg/ml, average, deviation and significance from supernatants of AMs of mice exposed to DM or BNNT-M and challenged with and without LPS is available as a supplement). Pre-treatment with BNNT-M and subsequent challenge with LPS drastically altered the cytokine profile in comparison to DM exposure with LPS challenge. These differentially expressed cytokines are known to play important roles in innate immunity (G-CSF, IL-1α, IL-1β, IFNγ, IP-10, GM-CSF, LIF and MCP-1) and adaptive immunity (IL-6, IL-4, IL-10 and RANTES). Apart from its effect on the immune system, differential expression of VEGF, IL-1α, GM-CSF and IL-6 suggests BNNT-M exposure followed by a secondary insult can have a profound effect on

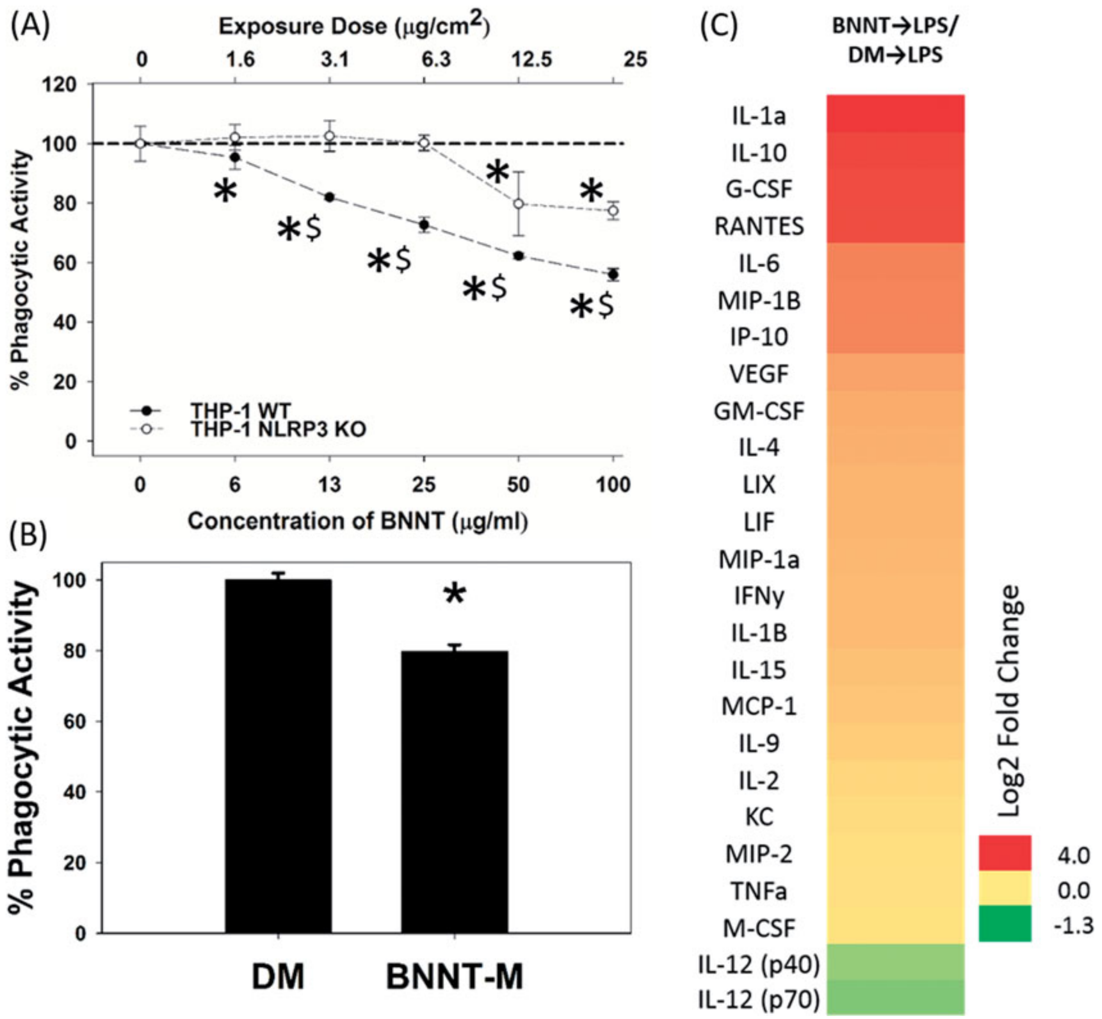

**Figure 6.** Modulation of macrophage cytokine profile and function after exposure to BNNT-M. (A) THP-1 WT and NLRP3-deficient macrophages were pretreated with indicated concentrations of BNNT-M for 24 h, followed by 2 h challenge with GFP *E. Coli* (MOI =25). Flow cytometry was used to measure bacterial uptake and was expressed as a percent of uptake relative to WT control. Pretreatment of BNNT-M caused a dose-dependent decrease in THP-1 WT macrophages ability to uptake bacteria. Except for the two highest doses tested, deficiency in NLRP3 protected the THP-1 cells from BNNT-M-induced dysfunction. (B) *Ex vivo*, alveolar macrophages collected from BALF of C57BL/6 mice exposed to BNNT-M (40 μg or ~0.08 μg/cm²) had a reduced ability to phagocytize bacteria compared to alveolar macrophages collected from DM-exposed mice, confirming our *in vitro* finding. (C) When challenged with LPS (1 ng/μl) for 12 h, alveolar macrophages collected from BNNT-M-exposed mice exhibited a varied phenotypical response compared to alveolar macrophages collected from DM exposed mice. *denotes statistical significance ($p < 0.05$) from DM-exposed animals (*in vivo*) or untreated cells (*in vitro*). $denotes statistical significance of THP-1 WT-exposed cells from equal mass exposed THP-1 NLRP3-deficient cells.

neovascularization and angiogenesis (Sunderkötter et al. 1994). These results illustrate that exposure to BNNT-M can cause dysregulation in macrophage responses to bacterial pathogens and may compromise a subsequent response to infections that may occur as a secondary exposure.

### In vitro *to* in vivo *correlation*

Recent dosimetric models provide significant improvements in estimating the effective *in vitro* exposure dose for a given *in vivo* exposure concentration (Hinderliter et al. 2010; Cohen Teeguarden, and Demokritou 2014; DeLoid et al. 2017). These models are primarily based on Stokes law to evaluate sedimentation and Stokes–Einstein equation for evaluating diffusion. Due to inherent limitation of these physical principles, these models are effective on spherical particles but cannot be used reliably for high aspect ratio particles like BNNTs or MWCNT-7. Currently, there is no known model for *in vitro* dosimetry of a high aspect ratio particulate. Most *in vitro* assays use an exposure concentration range of 0–100 μg/ml corresponding

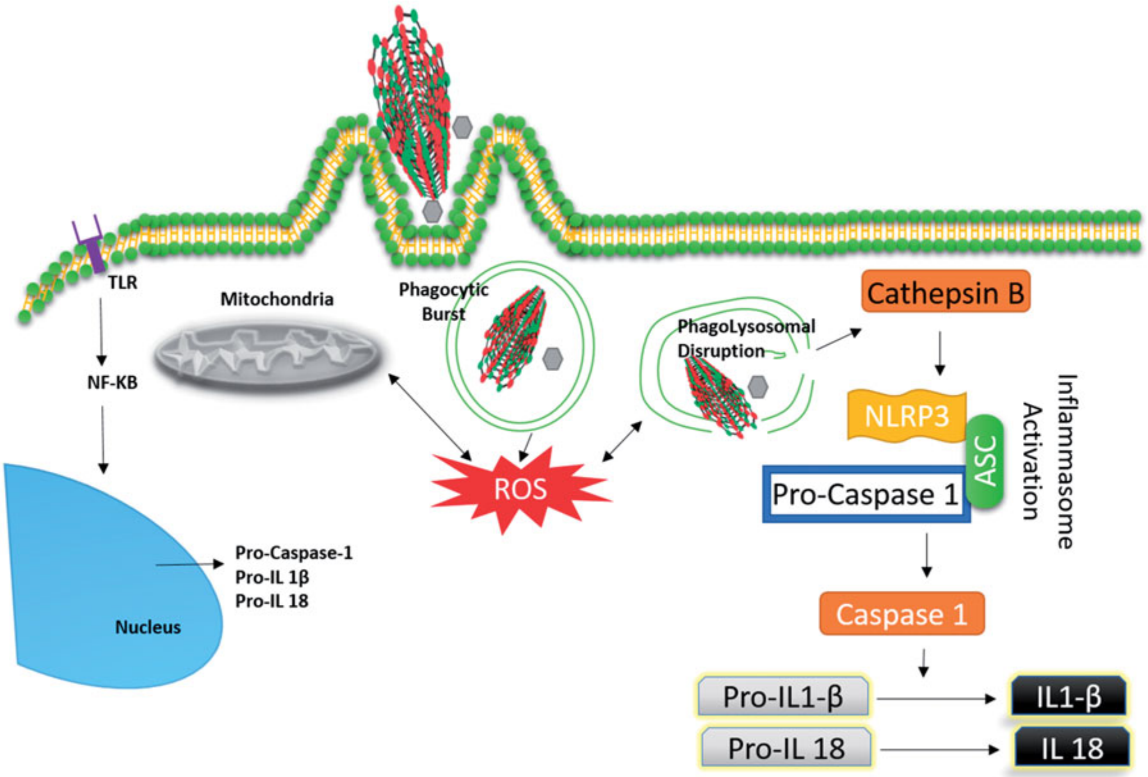

**Figure 7.** Proposed mechanism of NLRP3 inflammasome-dependent toxicity induced by BNNT-M exposure. Uptake of BNNT-M caused ROS production, mitochondrial dysfunction, and disruption in lysosomes integrity, thereby releasing active cathepsin B from lysosomes into the cytosol. Release of the lysosomal components triggered activation of NLRP3 inflammasome complex generating active caspase-1 and maturation of pro-IL-1β, pro-IL-18, ultimately secreting IL-1β, IL-18.

to a dose range of 0–31.25 μg/cm$^2$. Based on lung alveolar surface area of 500 cm$^2$/mouse (Stone et al. 1992; Wang et al. 2010) our *in vivo* exposure dose of 40 μg/mouse corresponds to 0.08 μg/cm$^2$, assuming all nanoparticles suspended in the culture media reach the cell surface. Although significant changes in toxicity, oxidative stress and inflammation were measured *in vivo* at this dose, at the corresponding *in vitro* dose of 0.08 μg/cm$^2$, there was no statistically significant change in any parameter measured. The discrepancy in sensitivity between *in vitro* and *in vivo* screens precludes us from conclusions based on absolute doses from *in vitro* experiments. The decrease in sensitivity can partially be attributed to the over simplistic assumption that all nanoparticles reached the cell surface and are engulfed by 24 h to initiate molecular signaling and the utilization of a single cell type as compared to more representative scenarios. As a significant portion of the nano-enabled product industry is based on high aspect ratio particles (e.g. carbon nanotubes), better dosimetric computational models for high aspect ratio particles are required to utilize *in vitro* screens. Though the absolute dose values from the *in vitro* screen were not useful for obtaining quantitative extrapolation of hazard, the excellent correlation between the *in vitro* and *in vivo* responses allowed us to use the *in vitro* model as a predictive screen and for understanding the mechanism of toxicity.

## *Occupational perspective*

Occupational exposure to various forms of boron have been reported in workers from manufacturing facilities of glass wool (Jensen 2009), ceramic factories (Roig-Navarro et al. 1997), mining and processing plants (Wegman et al. 1994). A 7-year human study at a U.S Mojave Desert plant site concluded that there was no statistically significant change in pulmonary function of workers exposed to various forms of boron derivatives (Wegman et al. 1994). Inhalation exposure of boron oxide up to 470 mg/m$^3$ in rats for 24 weeks or up to 57 mg/m$^3$ in dogs for 23 weeks showed no change in histopathology, liver function or systemic toxicity (Wilding et al.

1959). OSHA-permissible exposure limit for work place exposure for boron oxide is 15 mg/m$^3$ as a time-weighted average over an 8-h work day (ATSDR 2010). Exposure assessment studies to determine the levels of BNNT in occupational settings are not available to date and are currently being assessed by NIOSH at various occupational facilities. Exposure assessment studies performed on the morphologically similar MWCNT at eight U.S.-based MWCNT manufacturers showed an inhalable elemental carbon mass concentration arithmetic mean of 10.6 μg/m$^3$ (geometric mean 4.21 μg/m$^3$) in personal breathing zones of MWCNT workers, with approximately 20–25% of the inhalable fraction being respirable on average. (Erdely et al. 2013; Dahm et al. 2015) This concentration was equated to 2 ng/d in a mouse. Considering a normal working scenario of 8 hours/day, 5 days/week and 250 days/year, the dose that we administered, 40 μg/mouse, would be equivalent to a cumulative exposure of approximately 76 years (Erdely et al. 2013). At this point, similar extrapolations of the doses used in this study to exposure levels of the workplace cannot be performed due to lack of exposure assessment information in BNNT facilities. Using 15 mg/m$^3$, the exposure limits for boron oxide or total dust otherwise not regulated, or 1 μg/m$^3$, the recommended exposure limit for carbon nanotubes and nanofibers (NIOSH 2013), would create a discrepancy of several orders of magnitude. The dose we choose for our *in vivo* verification of the *in vitro* responses is known to cause MWCNT induced physiological and histopathological changes (Porter et al. 2010; Erdely et al. 2009). This exposure was intended for comparison with previously published data related to a structurally or categorically similar material (MWCNT-7). As such, the results from the current study are intended to provide a mechanistic perspective of the effects of BNNT-M exposure with respect to the well-studied MWCNT-7. The data further suggest a need for additional studies at occupationally relevant doses based on exposure assessment studies.

## Conclusions

The goal was to delineate a mechanism-based understanding of the acute toxicity induced by aqueous sonicated BNNT-M dispersion exposure *in vitro* and *in vivo*. The results demonstrated that BNNT-M, similar to MWCNT-7, induced inflammation *in vitro* and *in vivo* in part due to NLRP3 inflammasome activation. Based on the correlative data, the process may be initiated by lysosomal membrane permeabilization leading to release of cathepsin B and NLRP3 inflammasome activation. Inflammasome activation caused release of caspase-1 leading to pyroptosis and release of pro-inflammatory cytokines. The potential mechanism of BNNT-M induced inflammasome activation is depicted in Figure 7. The data suggest the tested BNNT-M was slightly less toxic than MWCNT-7 on an equal mass basis with regard to cytotoxicity, ROS generation, and elevation in pro-inflammatory cytokines like Il-1β. Pulmonary exposure to BNNT-M or MWCNT-7, at 40 μg per mouse, elicited an acute inflammatory response in mouse lungs characterized by rapid infiltration of polymorphonuclear cells and macrophages. Cytokines representing acute toxicity, as well as NLRP3 inflammasome activation and pyroptosis, were found to be elevated in the BALF. The close similarity in the acute toxicity profile of BNNT-M with the comparative high aspect ratio particle control MWCNT-7 suggests similarity in a categorical fashion. Functionally, BNNT-M exposure caused a suppression in macrophage phagocytic capacity both *in vitro* and *ex-vivo*. Apart from abrogation in this important protective function, LPS challenge experiments also showed that pre-exposure to BNNT-M altered macrophage cytokine profile suggesting a change in macrophages response.

BNNT-M used in the current study is prepared through a high temperature high pressure synthesis procedure from boron and nitrogen precursors. Annealing changes crystallinity and surface energy of the generated particles and this may have a profound effect on the toxicity induced by this material. The boron and hexagonal boron nitride impurities may or may not contribute to the observed toxicity; however, this was not investigated in present study. Further work is ongoing to delineate the toxicity of BNNTs from hexagonal boron/boron impurities present in the mixture. As applications and industrial use of BNNTs are increasing, exposure assessment studies are indispensable to better evaluate the health effects arising due to BNNTs/BNNT-M exposure related to occupational settings (Erdely et al. 2016) or in a life cycle scenario (Bishop et al. 2017) to provide relevant extrapolations to potential human health effects. Temporal studies are required to tease out if the acute toxicity observed persist across time and lead to adverse health outcomes. Based on the current results, sub-chronic *in vivo* studies over a wider occupationally-relevant dose range and time points are warranted to facilitate hazard ranking and risk assessment.

## Supporting information

Absolute values in pg/ml, average, deviation and significance of cytokine data from BAL Fluid of mice exposed to DM, BNNT-M or MWCNT-7 represented as heat map in Figure 5 is tabulated in supplemental information chart 1. Absolute values in pg/ml, average, deviation and significance of cytokine data from supernatants of AMs of mice exposed to DM or BNNT-M and challenged with and without LPS represented as heat map in Figure 6 is provided in supplemental information chart 2. This material is available free of charge via the Internet.

## Disclaimer

The findings and conclusions in this report are those of the authors and do not necessarily represent the views of the National Institute for Occupational Safety and Health.

## Disclosure statement

The authors Kodali, Roberts, Shoeb, Wolfarth, Bishop, Eye, Barger, Roach, Friend, Schwegler-Berry, Chen, Stefaniak, Porter and Erdely declare no competing conflict of interest. The authors Jordan and Whitney belong to BNNT LLC, a commercial manufacturer of Boron Nitride Nanotubes.

## Funding

This work was funded by the NIOSH Nanotechnology Research Center; 939011 M AE.

## References

Aragon, M. J., L. Topper, C. R. Tyler, B. Sanchez, K. Zychowski, T. Young, G. Herbert, et al. 2017. “Serum-Borne Bioactivity Caused by Pulmonary Multiwalled Carbon Nanotubes Induces Neuroinflammation via Blood–Brain Barrier Impairment.” *Proceedings of the National Academy of Sciences* 114: E1968–E1976.

Aragon, M., A. Erdely, L. Bishop, R. Salmen, J. Weaver, J. Liu, P. Hall, et al. 2016. “MMP-9-Dependent Serum-Borne Bioactivity Caused by Multiwalled Carbon Nanotube Exposure Induces Vascular Dysfunction via the CD36 Scavenger Receptor.” *Toxicological Sciences* 150: 488–498.

ATSDR. 2010. Toxicological profile for Boron. In: U.S. Department of Health and Human Services, PHS ed. Atlanta, GA: Agency for Toxic Substances and Disease Registry.

Bergsbaken, T., S. L. Fink, and B. T. Cookson. 2009. “Pyroptosis: Host Cell Death and Inflammation.” *Nature Reviews Microbiology* 7: 99–109.

Bishop, L., L. Cena, M. Orandle, N. Yanamala, M. M. Dahm, M. E. Birch, D. E. Evans, et al. 2017. “In Vivo Toxicity Assessment of Occupational Components of the Carbon Nanotube Life Cycle To Provide Context to Potential Health Effects.” *ACS Nano* 11: 8849–8863.

Cassel, S. L., S. C. Eisenbarth, S. S. Iyer, J. J. Sadler, O. R. Colegio, L. A. Tephly, A. B. Carter, et al. 2008. “The Nalp3 Inflammasome is Essential for the Development of Silicosis.” *Proceedings of the National Academy of Sciences of the United States of America* 105: 9035–9040.

Chen, B. T., D. Schwegler-Berry, W. McKinney, S. Stone, J. L. Cumpston, S. Friend, D. W. Porter, et al. 2012. “Multi-Walled Carbon Nanotubes: Sampling Criteria and Aerosol Characterization.” *Inhalation Toxicology* 24: 798–820.

Chen, X., P. Wu, M. Rousseas, D. Okawa, Z. Gartner, and C. R. Bertozzi. 2009. “Boron Nitride Nanotubes are Noncytotoxic and can be Functionalized for Interaction with Proteins and Cells.” *Journal of the American Chemical Society* 131: 890–891.

Ciofani, G., S. Danti, D. D’Alessandro, S. Moscato, and A. Menciassi. 2010. “Assessing Cytotoxicity of Boron Nitride Nanotubes: Interference with the MTT Assay.” *Biochemical and Biophysical Research Communications* 394: 405–411.

Cohen, J. M., J. G. Teeguarden, and P. Demokritou. 2014. “An Integrated Approach for the In Vitro Dosimetry of Engineered Nanomaterials.” *Particle and Fibre Toxicology* 11: 20.

Dahm, M. M., M. K. Schubauer-Berigan, D. E. Evans, M. E. Birch, J. E. Fernback, and J. A. Deddens. 2015. “Carbon Nanotube and Nanofiber Exposure Assessments: An Analysis of 14 Site Visits.” *Annals of Occupational Hygiene* 59: 705–723.

DeLoid, G. M., J. M. Cohen, G. Pyrgiotakis, and P. Demokritou. 2017. “Preparation, Characterization, and In Vitro Dosimetry of Dispersed, Engineered Nanomaterials.” *Nature Protocols* 12: 355–371.

Dong, J., and Q. Ma. 2015. “Advances in Mechanisms and Signaling Pathways of Carbon Nanotube Toxicity.” *Nanotoxicology* 9: 658–676.

Dostert, C., V. Pétrilli, R. Van Bruggen, C. Steele, B. T. Mossman, and J. Tschopp. 2008. “Innate Immune Activation Through Nalp3 Inflammasome Sensing of Asbestos and Silica.” *Science (New York, N.Y.)* 320: 674–677.

Duan, J., V. K. Kodali, M. J. Gaffrey, J. Guo, R. K. Chu, D. G. Camp, R. D. Smith, et al. 2015. “Quantitative Profiling of Protein S-Glutathionylation Reveals Redox-Dependent Regulation of Macrophage Function during Nanoparticle-Induced Oxidative Stress.” *ACS Nano* 10: 524–538.

Erdely, A., M. Dahm, B. T. Chen, P. C. Zeidler-Erdely, J. E. Fernback, M. E. Birch, D. E. Evans, et al. 2013. “Carbon Nanotube Dosimetry: From Workplace Exposure Assessment to Inhalation Toxicology.” *Particle and Fibre Toxicology* 10: 53.

Erdely, A., M. M. Dahm, M. K. Schubauer-Berigan, B. T. Chen, J. M. Antonini, and M. D. Hoover. 2016. “Bridging the gap between exposure assessment and inhalation toxicology: Some insights from the carbon nanotube experience.” *Journal of Aerosol Science* 99: 157–162.

Erdely, A., T. Hulderman, R. Salmen, A. Liston, P. C. Zeidler-Erdely, D. Schwegler-Berry, V. Castranova, et al. 2009. “Cross-Talk Between Lung and Systemic Circulation During Carbon Nanotube Respiratory Exposure.” *Potential Biomarkers. Nano Letters* 9: 36–43.

Ferreira, T. H., P. Silva, R. Santos, and E. Sousa. 2011. “A Novel Synthesis Route to Produce Boron Nitride Nanotubes for Bioapplications.” *Journal of Biomaterials and Nanobiotechnology* 2: 426.

Ge, C., Y. Li, J. J. Yin, Y. Liu, L. Wang, Y. Zhao, and C. Chen. 2012. “The Contributions of Metal Impurities and Tube Structure to the Toxicity of Carbon Nanotube Materials.” *NPG Asia Materials* 4: e32.

Godwin, H., C. Nameth, D. Avery, L. L. Bergeson, D. Bernard, E. Beryt, W. Boyes, et al. 2015. “Nanomaterial Categorization for Assessing Risk Potential to Facilitate Regulatory Decision-Making.” *ACS Nano* 9: 3409–3417.

Guo, H., J. B. Callaway, and J. P. Ting. 2015. “Inflammasomes: Mechanism of Action, Role in Disease, and Therapeutics.” *Nature Medicine* 21: 677–687.

Hamilton, R. F., Z. Wu, S. Mitra, P. K. Shaw, and A. Holian. 2013. “Effect of MWCNT Size, Carboxylation, and Purification on In Vitro and In Vivo Toxicity, Inflammation and Lung Pathology.” *Particle and Fibre Toxicology* 10.

Hinderliter, P. M., K. R. Minard, G. Orr, W. B. Chrisler, B. D. Thrall, J. G. Pounds, and J. G. Teeguarden. 2010. “ISDD: A Computational Model of Particle Sedimentation, Diffusion and Target Cell Dosimetry for In Vitro Toxicity Studies.” *Particle and Fibre Toxicology* 7: 36.

Horvath, L., A. Magrez, D. Golberg, C. Zhi, Y. Bando, R. Smajda, E. Horvath, et al. 2011. “In Vitro Investigation of the Cellular Toxicity of Boron Nitride Nanotubes.” *ACS Nano* 5:3800–3810.

Jensen, A. A. 2009. “Risk Assessment of Boron in Glass Wool Insulation.” *Environmental Science and Pollution Research International* 16: 73–78.

Jiang, Y., H. Zhang, Y. Wang, M. Chen, S. Ye, Z. Hou, and L. Ren. 2013. “Modulation of Apoptotic Pathways of Macrophages by Surface-Functionalized Multi-Walled Carbon Nanotubes.” *PLoS One* 8: e65756.

Johnston, H. J., G. R. Hutchison, F. M. Christensen, S. Peters, S. Hankin, K. Aschberger, and V. Stone. 2010. “A Critical Review of the Biological Mechanisms Underlying the In Vivo and In Vitro Toxicity of Carbon Nanotubes: The Contribution of Physico-Chemical Characteristics.” *Nanotoxicology* 4: 207–246.

Kodali, V., and B. D. Thrall. 2015. “Oxidative Stress and Nanomaterial-Cellular Interactions.” In: *Studies on Experimental Toxicology and Pharmacology*, edited by M. S. Roberts, P. J. Kehrer, and L.-O. Klotz, 347–367. Cham: Springer International Publishing.

Kodali, V., M. H. Littke, S. C. Tilton, J. G. Teeguarden, L. Shi, C. W. Frevert, W. Wang, et al. 2013. “Dysregulation of Macrophage Activation Profiles by Engineered Nanoparticles.” *ACS Nano* 7: 6997–7010.

Kuempel, E. D., V. Castranova, C. L. Geraci, and P. A. Schulte. 2012. “Development of Risk-Based Nanomaterial Groups for Occupational Exposure Control.” *Journal of Nanoparticle Research* 14: 1029.

Labib, S., A. Williams, C. L. Yauk, J. K. Nikota, H. Wallin, U. Vogel, S. Halappanavar. 2016. “Nano-Risk Science: Application of Toxicogenomics in an Adverse Outcome Pathway Framework for Risk Assessment of Multi-Walled Carbon Nanotubes.” *Particle and Fibre Toxicology* 13:15.

Mercer, R. R., J. F. Scabilloni, A. F. Hubbs, L. A. Battelli, W. McKinney, S. Friend, M. G. Wolfarth, et al. 2013. “Distribution and Fibrotic Response Following Inhalation Exposure to Multi-Walled Carbon Nanotubes.” *Particle and Fibre Toxicology* 10: 33.

Miao, E. A., J. V. Rajan, and A. Aderem. 2011. “Caspase-1-Induced Pyroptotic Cell Death.” *Immunological Reviews* 243: 206–214.

National Research Council. 2011. *Guide for the Care and Use of Laboratory Animals*. Washington, DC: National Academies Press.

NIH. 1986. *Public Health Service Policy on Humane Care and Use of Laboratory Animals*. Bethesda, MD: National Institutes of Health (U.S.A).

NIOSH. 2013. *Current Intelligence Bulletin 65: Occupational Exposure to Carbon Nanotubes and Nanofibers*. DHHS (NIOSH) Publication.

Nymark, P., P. Wijshoff, R. Cavill, M. van Herwijnen, M. L. Coonen, S. Claessen, J. Catalán, et al. 2015. “Extensive Temporal Transcriptome and MicroRNA Analyses Identify Molecular Mechanisms Underlying Mitochondrial Dysfunction Induced by Multi-Walled Carbon Nanotubes in Human Lung Cells.” *Nanotoxicology* 9: 624–635.

Oberdörster, G., V. Castranova, B. Asgharian, and P. Sayre. 2015. “Inhalation Exposure to Carbon Nanotubes (CNT) and Carbon Nanofibers (CNF): Methodology and Dosimetry.” *Journal of Toxicology and Environmental Health, Part B* 18: 121–212.

Pope, C III. 2000. “Epidemiology of Fine Particulate Air Pollution and Human Health: Biologic Mechanisms and Who's at Risk?” *Environmental Health Perspectives* 108: 713.

Porter, D. W., A. F. Hubbs, B. T. Chen, W. McKinney, R. R. Mercer, M. G. Wolfarth, L. Battelli, et al. 2012. “Acute Pulmonary Dose–Responses to Inhaled Multi-Walled Carbon Nanotubes.” *Nanotoxicology* 7: 1179–1194.

Porter, D. W., A. F. Hubbs, R. R. Mercer, N. Wu, M. G. Wolfarth, K. Sriram, S. Leonard, et al. 2010. “Mouse Pulmonary Dose-and Time Course-Responses Induced by

Exposure to Multi-Walled Carbon Nanotubes." *Toxicology* 269: 136–147.

Porter, D., K. Sriram, M. Wolfarth, A. Jefferson, D. Schwegler-Berry, M. E. Andrew, and V. Castranova. 2008. "A Biocompatible Medium for Nanoparticle Dispersion." *Nanotoxicology* 2: 144–154.

Rasel, M. A. I., T. Li, T. D. Nguyen, S. Singh, Y. Zhou, Y. Xiao, and Y. Gu. 2015. "Biophysical Response of Living Cells to Boron Nitride Nanoparticles: Uptake Mechanism and Bio-Mechanical Characterization." *Journal of Nanoparticle Research* 17: 441.

Rocca, A., A. Marino, S. Del Turco, V. Cappello, P. Parlanti, M. Pellegrino, D. Golberg, et al. 2016. "Pectin-Coated Boron Nitride Nanotubes: In vitro Cyto-/Immune-Compatibility on RAW 264.7 Macrophages." *Biochimica Et Biophysica Acta (BBA)-General Subjects* 1860: 775–784.

Roco, M. C., C. A. Mirkin, and M. C. Hersam. 2011. *Nanotechnology Research Directions for Societal Needs in 2020: Retrospective and Outlook*. New York: Springer Science & Business Media.

Roig-Navarro, A. F., F. J. López, R. Serrano, and F. Hernández. 1997. "An Assessment of Heavy Metals and Boron Contamination in Workplace Atmospheres from Ceramic Factories." *Science of the Total Environment* 201: 225–234.

Sargent, L. M., D. W. Porter, L. M. Staska, A. F. Hubbs, D. T. Lowry, L. Battelli, K. J. Siegrist, et al. 2014. "Promotion of Lung Adenocarcinoma Following Inhalation Exposure to Multi-Walled Carbon Nanotubes." *Particle and Fibre Toxicology* 11: 3.

Schwartz, J., D. W. Dockery, and L. M. Neas. 1996. "Is Daily Mortality Associated Specifically with Fine Particles?" *Journal of the Air and Waste Management Association* 46: 927–939.

Shvedova, A. A., A. Pietroiusti, B. Fadeel, and V. E. Kagan. 2012. "Mechanisms of Carbon Nanotube-Induced Toxicity: Focus on Oxidative Stress." *Toxicology and Applied Pharmacology* 261: 121–133.

Smith, M. W., K. C. Jordan, C. Park, J. W. Kim, P. T. Lillehei, R. Crooks, and J. S. Harrison. 2009. "Very Long Single-and Few-Walled Boron Nitride Nanotubes Via the Pressurized Vapor/Condenser Method." *Nanotechnology* 20: 505604.

Stern, S. T., P. P. Adiseshaiah, and R. M. Crist. 2012. "Autophagy and Lysosomal Dysfunction as Emerging Mechanisms of Nanomaterial Toxicity." *Particle and Fibre Toxicology* 9: 20.

Stone, K. C., R. R. Mercer, B. A. Freeman, L.-Y. Chang, and J. D. Crapo. 1992. "Distribution of Lung Cell Numbers and Volumes Between Alveolar and Nonalveolar Tissue." *American Review of Respiratory Disease* 146: 454–456.

Sun, B., X. Wang, Z. Ji, M. Wang, Y. P. Liao, C. H. Chang, R. Li, et al. 2015. "NADPH Oxidase-Dependent NLRP3 Inflammasome Activation and its Important Role in Lung Fibrosis by Multiwalled Carbon Nanotubes." *Small* 11: 2087–2097.

Sun, B., X. Wang, Z. Ji, R. Li, and T. Xia. 2013. "NLRP3 Inflammasome Activation Induced by Engineered Nanomaterials." *Small* 9: 1595–1607.

Sunderkötter, C., K. Steinbrink, M. Goebeler, R. Bhardwaj, and C. Sorg. 1994. "Macrophages and Angiogenesis." *Journal of Leukocyte Biology* 55: 410–422.

Tsuruoka, S., F. R. Cassee, and V. Castranova. 2013a. "A New Approach to Design Safe CNTs with an Understanding of Redox Potential." *Particle and Fibre Toxicology* 10: 44.

Tsuruoka, S., K. Takeuchi, K. Koyama, T. Noguchi, M. Endo, F. Tristan, M. Terrones, et al. 2013b. "ROS Evaluation for a Series of CNTs and their Derivatives using an ESR Method with DMPO." *Journal of Physics: Conference Series* 429: 12029.

Vietti, G., D. Lison, and S. van den Brule. 2016. "Mechanisms of Lung Fibrosis Induced by Carbon Nanotubes: Towards an Adverse Outcome Pathway (AOP)." *Particle and Fibre Toxicology* 13:11.

Villeneuve, D. L., D. Crump, N. Garcia-Reyero, M. Hecker, T. H. Hutchinson, C. A. LaLone, B. Landesmann, et al. 2014. "Adverse Outcome Pathway (AOP) Development I: Strategies and Principles." *Toxicological Sciences* 142:312–320.

Wang, L., V. Castranova, A. Mishra, B. Chen, R. R. Mercer, D. Schwegler-Berry, and Y. Rojanasakul. 2010. "Dispersion of Single-Walled Carbon Nanotubes by a Natural Lung Surfactant for Pulmonary In Vitro and In Vivo Toxicity Studies." *Particle and Fibre Toxicology* 7: 31.

Wegman, D. H., E. A. Eisen, X. Hu, S. R. Woskie, R. G. Smith, and D. H. Garabrant. 1994. "Acute and Chronic Respiratory Effects of Sodium Borate Particulate Exposures." *Environmental Health Perspectives* 102: 119–128.

Wilding, J. L., W. J. Smith, P. Yevich, M. E. Sicks, S. G. Ryan, and C. L. Punte. 1959. "The Toxicity of Boron Oxide." *American Industrial Hygiene Association Journal* 20: 284–289.

Xia, T., R. F. Hamilton, Jr., J. C. Bonner, E. D. Crandall, A. Elder, F. Fazlollahi, T. A. Girtsman, et al. 2013. "Interlaboratory Evaluation of In Vitro Cytotoxicity and Inflammatory Responses to Engineered Nanomaterials: The NIEHS Nano GO Consortium." *Environmental Health Perspectives* 121: 683.

Zeidler-Erdely, P. C., A. Erdely, and J. M. Antonini. 2012. "Immunotoxicology of Arc Welding Fume: Worker and Experimental Animal Studies." *Journal of Immunotoxicology* 9: 411–425.

Zhang, H., Z. Ji, T. Xia, H. Meng, C. Low-Kam, R. Liu, S. Pokhrel, et al. 2012. "Use of Metal Oxide Nanoparticle Band Gap to Develop a Predictive Paradigm for Oxidative Stress and Acute Pulmonary Inflammation." *ACS Nano* 6: 4349–4368.